Superconducting Nanowires Templated by Single Molecules

Alexey Bezryadin
University of Illinios at Urbana-Champaign, Champaign, Illinois, U.S.A.

Anthony Bollinger
David Hopkins
Michael Murphey
Mikas Remeika
Andrey Rogachev
University of Illinois at Urbana-Champaign, Urbana, Illinois, U.S.A.

INTRODUCTION

Ultrathin superconducting nanowires (SNWs) can be classified as ''weak superconducting links''.[1] They have properties in many ways similar to Josephson junctions. Thus, SNWs can find possible applications in superconducting information processing devices: either classical[2,3] or quantum.[4–7] Nanowires can also be used as detectors and mixers of microwave radiation.[8,9] Fundamentally, the SNW is a model system for understanding coherence and decoherence effects, quantum phase transitions, and macroscopic quantum tunneling phenomena in one-dimensional (1-D) superfluids.[10–21]

Because of the strong thermal fluctuations in 1-D, the resistance of a nanowire cannot be zero at any finite temperature. The limit of zero temperature is governed by quantum fluctuations, which are not well understood. Therefore, SNWs can fall into one of three different categories: 1) truly superconducting, i.e., with zero resistance in the limit of zero temperature, 2) resistive or normal, with a nonzero but finite resistance (R) at zero temperature (T), and 3) insulating, with $R\rightarrow\infty$ as $T\rightarrow 0$. On general grounds, it is expected that extremely thin nanowires should lose their ability to carry a supercurrent. General conditions under which this happens are not known. Many experiments show that nanowires having their normal state resistance, R_N, lower than the superconducting quantum resistance, $R_Q=h/(2e)^2\approx 6.5\ \mathrm{k\Omega}$, obey the predictions of the Langer, Ambegaokar, McCumber, and Halperin (LAMH) theory of thermally activated phase slips (TAPS). Such wires can be considered true superconductors because this theory predicts zero resistance at zero temperature. On the other hand, SNWs with $R_N>R_Q$ frequently show deviations from LAMH or even an insulating behavior.[11] In some cases, these deviations can be explained by the effect of quantum phase slips (QPS).[12]

Here we focus on superconducting nanowires produced by sputter-coating single linear molecules (carbon nanotubes, DNA) with thin metallic films. Such molecular templating technique[11] results in nanowires that are thinner than 10 nm in diameter. Continuous SNWs were produced with the following two materials:[11,12,22] 1) amorphous alloy of MoGe, which is usually used for making extremely thin (down to $\sim$1.5 nm) and homogeneous films,[23–25] and 2) Nb metal, which finds applications in superconducting electronic circuits. Although Nb wires are polycrystalline,[22] the critical current density in them is $\sim 10^7$ A/cm^2, i.e., is similar to bulk practical superconductors (Ref. [26] p. 372).

PROPERTIES OF SUPERCONDUCTING NANOWIRES

Thermally Activated Phase Slips

The physics of superconducting nanowires is extremely rich and many puzzles remain unresolved. Perhaps the most striking property of SNWs is their inability to reach zero resistance at any nonzero temperature.[27] This property agrees with the Mermin–Wagner theorem,[28] which prohibits thermodynamic phase transitions in 1-D systems.[a] In particular, a thin 1-D wire made of a superconducting metal cannot undergo a phase transition into a fully superconducting state, i.e., a state with $R=0$ at any nonzero temperature. The mechanism of acquiring a nonzero resistance is known as phase slippage (PS) process. It is due to strong thermal (or possibly quantum)

[a]A superconducting nanowire is considered 1-D if the diameter of the wire is the same as the superconducting coherence length or smaller.

DOI: 10.1081/E-ENN 120013540

fluctuations in 1-D wires.[29] The theory of thermally activated phase slips (TAPS) was developed by Langer, Ambegaokar, McCumber, and Halperin (LAMH).[30,31] Thermally activated phase slips have been studied since the 70s and are quite well understood. Early experiments on 0.5-μm-diameter tin whiskers confirmed the LAMH theory.[32,33]

Each TAPS is a strong and short-lasting thermodynamic fluctuation occurring in a short segment of length, $\sim 2\xi(T)$, somewhere along the wire. The order parameter, $\psi = |\psi| e^{i\varphi}$, is zero [$\psi(x,t)=0$] at the center of the TAPS and, correspondingly, the phase, $\varphi(x,t)$, is indeterminate at this point. So, with each TAPS the phase difference $\Delta\varphi = \varphi(L) - \varphi(0)$ along the wire changes by $\pm 2\pi$. Here x is the position along the wire and L is the wire length. In the absence of phase slips, a state of constant supercurrent, $\psi(x) = |\psi| e^{ikx}$, is realized. The wave vector, k, is proportional to the supercurrent, I_S. The amplitude, $|\psi|$, is constant along the wire if I_S=constant. A convenient presentation of $\psi(x)$ is given in Fig. 1. Here two axes correspond to the real and imaginary parts of $\psi(x)$, and the third axis is the space coordinate x. In this representation a spiral of a constant radius represents a state with I_S=constant. The number of turns in the spiral is proportional to I_S. Thus, if the winding number does not change then the current remains constant. On the other hand, if a phase slip occurs, the order parameter goes to zero at one point and the spiral loses one loop, so the supercurrent diminishes. A phase slip (PS) event is shown in Fig. 1. An antiphase slip (APS) is a similar fluctuation that increases the winding number by one. Thus, the phase difference between the ends of the wire changes by -2π for each PS and by $+2\pi$ for each APS.

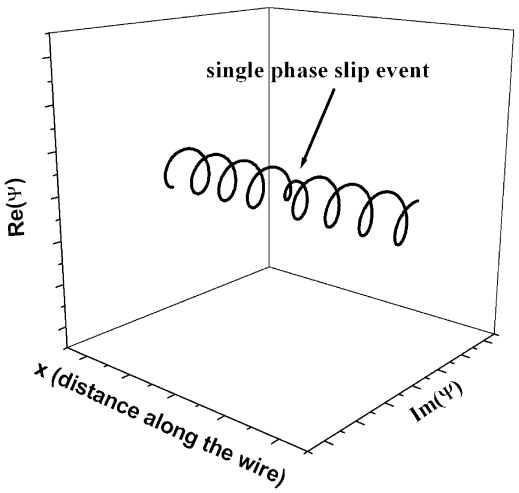

Fig. 1 Superconducting order parameter of a thin wire with a phase slip (PS) in the center. The PS is a short-lived event ($\sim 10^{-12}$ sec) during which the order parameter goes to zero at one point. During the PS, the spiral loses one loop and the supercurrent becomes smaller.

The problem of calculating the resistance reduces to finding the rate at which phase slips occur in the nanowire. The voltage on the wire (at a fixed small bias current, I) is given by the Josephson relation $2eV = \hbar(d\varphi/dt) = 2\pi(n_+ - n_-)\hbar \equiv 2\pi\hbar\Delta n$, where n_+ and n_- are the rates of PS and APS, respectively. The predicted volume of the phase slip is $V_{PS} \approx 3.77\xi A$, where A is the cross section area of the wire.[30] The free energy of a PS is $\Delta F(T) = [H_C^2(T)/8\pi]V_{PS}$, where $H_C(T)$ is the thermodynamic critical field. At zero bias current, $I=0$, the rates of PS and APS are equal: $n_+ - n_- = n = \Omega \exp[-\Delta F(T)/k_B T]$, where $\Omega = [8k_B(T_C - T)/\pi\hbar][L/\xi(T)]\sqrt{\Delta F/kT}$ is the so-called attempt frequency, k_B the Boltzmann constant, $\hbar$ Planck's constant, T the temperature, and T_C the critical temperature. At $I>0$ the barrier corresponding to PS is lower than the APS one, leading to a net phase flow, $n_+ > n_-$. We have $n_\pm = \Omega \exp[-(\Delta F(T) \pm \delta F)/k_B T]$ and $\Delta n = 2\Omega \exp[-\Delta F(T)/k_B T] \sinh(\delta F/kT)$, where $\delta F = \pi\hbar I/2e$ is half of the free energy difference between PS and APS. Using the relation $R = dV/dI = (\pi\hbar/e)d(\Delta n)/dI$ one gets the following resistance vs. temperature dependence (here $t = T/T_C$):

$$R_{LAMH}(T) = Dt^{-3/2}(1-t)^{9/4} \exp\left[\frac{-c}{t}(1-t)^{3/2}\right] \tag{1}$$

Because of the normal quasiparticles present in the wire close to T_C,[27] the final expression for the wire's resistance, $R(T)$, is:

$$R^{-1} = R_{LAMH}^{-1} + R_N^{-1} \tag{1a}$$

where R_N is the normal-state resistance of the wire. The LAMH defines the constants D and c as follows:[12]

$$c \equiv \frac{\Delta F(0)}{kT_C} = \frac{1.76\sqrt{2}}{3}\frac{R_Q}{R_N}\frac{L}{\xi(0)} \tag{2}$$

and

$$D = (8/\pi)[L/\xi(0)]R_Q\sqrt{c} \tag{3}$$

where $\xi(0)$ is zero temperature coherence length [$\xi(0) \approx 7$ nm for MoGe samples].

Quantum Phase Slips

Two types of phase slips are usually distinguished: TAPS, discussed above, and QPS. The QPS can be observed only in very thin wires, about 10 nm in diameter or less.[14] Such nanowires can be made using the technique of suspended molecular templates (SMT).[11] The SMT

method is unique because it results in nanowires that are not only very thin (down to ~3 nm) but also can be made very short, less than 100 nm if necessary. This length is comparable to or shorter than the electronic inelastic mean free path $L_i = \sqrt{D\tau_i} \simeq 100$–$1000$ nm (here $D = lv_F/3 \sim 10^{-3}$–10^{-4} m^2 sec is the diffusion constant and $\tau_i \sim 10^{-9}$–10^{-10} sec is the inelastic scattering time). The electrons in such short SNWs can diffuse through the entire wire without undergoing inelastic collision, and so they are able to preserve quantum phase information.

The possibility of quantum tunneling of phase slips attracts much attention because QPS can be regarded as a macroscopic quantum phenomenon. On general grounds, it is expected that the probability of quantum phase slips should be proportional to $\exp[-\Delta F(0)/\hbar\omega_S]$, where $\hbar$ is the Planck's constant and ω_S is some characteristic frequency of quantum fluctuations of the superconducting order parameter. A semiquantitative model of quantum phase slips was suggested by Giordano.[10] Recent experiments on MoGe wires showed good agreement with Giordano's model[12] (see discussion below). The QPS contribution is explained in detail in Ref. [12] The expression for the resistance in the case of QPS is similar to Eq. 1a but an additional term is added that represents the contribution of the macroscopic quantum tunneling (MQT) of the phase slips (i.e., the contribution of QPS):

$$R^{-1} = (R_{MQT} + R_{LAMH})^{-1} + R_N^{-1} \quad (4)$$

Here $R_{MQT} = \rho_{QC} R_{LAMH}$ and $\rho_{QC} = B[\pi t/8(1-t)]^{3/2} \exp[c\sqrt{1-t}((1-t)/t - a\pi/8)]$. The coefficients a and B are the two fitting parameters. These formulas are equivalent to those used in Ref. [12] Here we explicitly introduce the temperature-dependent ratio $\rho_{QC} \equiv R_{MQT}/R_{LAMH}$. By using the formulas from Ref. [12] it can be shown that the ρ_{QC} ratio is larger than unity (meaning that quantum tunneling of phase slips occurs with a higher rate than the thermal activation) if the temperature is $T < 0.7T_C$. This ratio of the quantum and thermal contributions (i.e., ρ_{QC}) is plotted in Fig. 8 (inset).

QPS and TAPS have different implications. If only TAPS is present, then the wire is classified as ''truly superconducting'' in the sense that its resistance approaches zero as the temperature approaches zero. If QPS is also present, the resistance stays above zero even in the limit of zero temperature so the wire remains restive or normal. Thus, TAPS is responsible for breaking superconductivity at finite temperature and QPS destroys superconductivity in the limit of zero temperature. The existence of QPS is regarded as a limiting factor for miniaturization of superconducting devices.[34] Under certain conditions, a proliferation of QPS can suppress superconductivity and can cause a superconductor–insulator (SI) quantum transition.[11,14–16]

FABRICATION OF SUPERCONDUCTING NANOWIRES

Molecular Templating with Nanotubes

The suspended molecular templates (SMT) method[11] uses suspended, linear rigid molecules as templates for metal coating. Three types of molecules have been tested: 1) ordinary single-wall carbon nanotubes,[11,12] fluorinated carbon nanotubes,[35,36] which are 100% insulating, and DNA molecules (see below). Because these molecules are very thin, 1–3 nm in diameter, the resulting nanowires can be made thinner than 10 nm. It was found that MoGe wires made on insulating fluorotubes have similar properties to those made on regular nanotubes. Thus the nanotube does not contribute significantly to the total conductance of the wire. Note that suspended nanotubes can also be used for the fabrication of magnetic nanowires.[37]

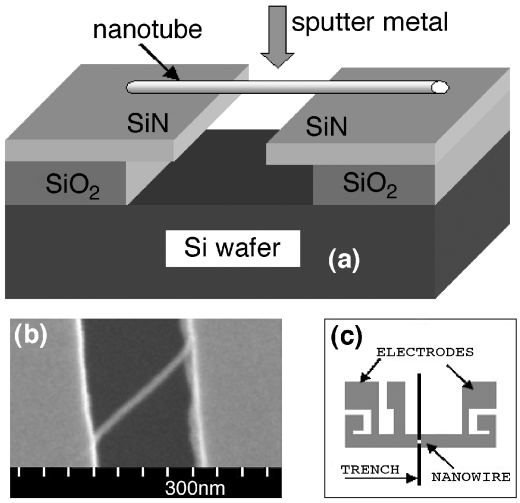

Fig. 2 The sample schematics. (a) The nanotubes are deposited over a trench, and a superconducting metal (Nb or MoGe) is sputtered over the entire surface of the Si chip. Thus the electrodes are formed on the banks of the trench and, at the same time, suspended nanowires form with nanotubes in their cores. Because the sample is sputtered only once, the wires have the same thickness as the electrodes. In addition, the wires are seamlessly connected to the electrodes, without any unwanted contact barrier. Photolithography and reactive ion etching are subsequently used to define the shape of the electrodes and destroy all wires but one. The d.c. sputtering is done in an argon atmosphere, in a sputtering chamber equipped with a cryogenic liquid nitrogen trap. (b) A scanning electron micrograph of a nanowire (gray line) suspended over a trench (black) and connecting to two MoGe electrodes (gray areas). (c) Schematic top view of the sample. The size of the Si chip is 5×5 mm. (*View this art in color at www.dekker.com.*)

The SMT technique is described in detail in Ref. [11] The fabrication process starts with an Si(100) wafer covered with a layer of 500-nm-thick SiO_2 and 60-nm-thick film of low-stress SiN.[38] A narrow and very long trench is then defined in the SiN film using e-beam lithography and reactive ion etching in SF_6 plasma. The resulting trench (Fig. 2) has a width of $\sim$100 nm and length of $\sim$5 mm. An undercut is then formed by placing the sample in HF for 10 sec.

Fluorinated nanotubes are deposited from a solution in isopropyl alcohol. After drying, the sample is sputter-coated with the desired superconducting metal, typically $\sim$4–8 nm of $Mo_{79}Ge_{21}$ (Fig. 2a). After sputtering, each nanotube suspended over the trench becomes decorated with metal and thus forms a metallic nanowire. A nanowire of desired width is then selected under scanning electron microscopy (SEM) (Fig. 2b) and photolithography is used for making the electrodes and etching all nanowires except the selected one (Fig. 2c).

Molecular Templating with DNA

The DNA molecule is of course not as rigid as a carbon nanotube. Nevertheless, it is observed that when being suspended, the DNA stretches itself. Thus, DNA provides an excellent molecular template for metal deposition. For example, the micrograph in Fig. 3a shows six metal-coated DNA wires, which are visible as thin gray lines of length $\sim$150 nm. The tests were done on the same type of $Si/SiO_2/SiN$ substrate with trenches made as described earlier. The λ-DNA molecules have been deposited over the oxygen-plasma-cleaned SiN surface from a buffer solution with a 40 μg/mL concentration. The samples were then dried and metal coated. Two important conclusions can be drawn from these experiments: 1) Because of some intrinsic mechanism, the suspended DNA molecules become stretched and appear very straight. 2) Many metals, such as Os, Cr, and MoGe, showed good adhesion to the DNA surface and produced visibly homogeneous wires. A coating of DNA with a thin ($\sim$3nm) AuPd film produced granular wires (Fig. 3b). The fact that DNA appears so straight is somewhat unexpected because DNA is not nearly as rigid as carbon nanotubes. A possible explanation is that DNA interacts attractively with the substrate due to the van der Waals force. Thus, it is energetically favorable for the molecule to minimize the length of the freely suspended section. So, the suspended part becomes strained and perfectly straight.

Morphology of Nb and MoGe Nanowires

The morphology of nanowires was determined using transmission electron microscopy (TEM).[22] The wires

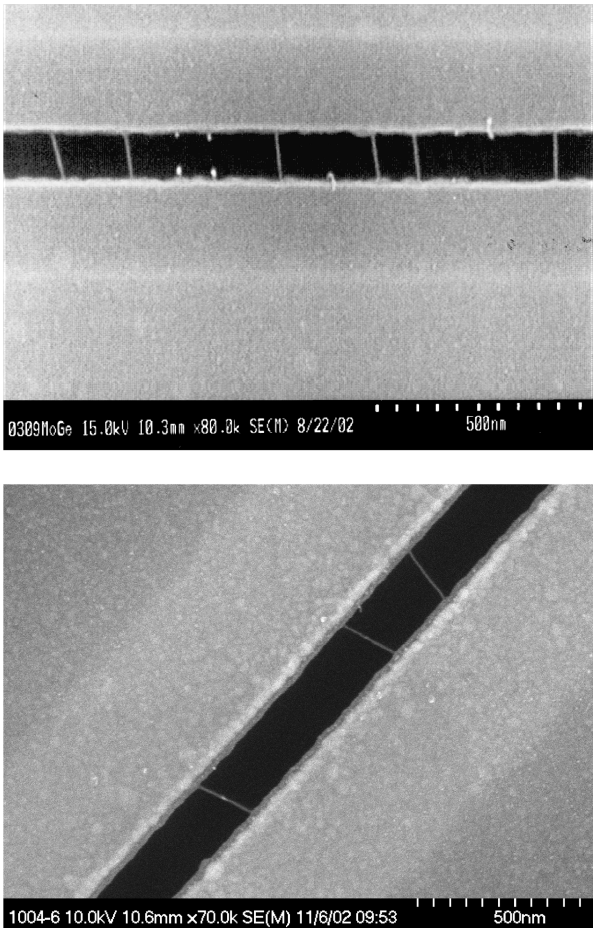

Fig. 3 Metal decoration of suspended DNA molecules. The black region is the trench with an undercut. Nanowires appear as thin gray lines crossing the trench. The sample (a) has six surviving nanowires. λ-DNA molecules were deposited from a buffer dilute solution, dried, and sputter-coated with 4 nm of MoGe and 3 nm of SiO_2. (b) Nanowires of gold–palladium templated by DNA. The trench was cut into SiN film using a focused ion beam. A 50-nm-thick gold film was deposited before the application of DNA. After the λ-DNA deposition, the sample was sputter-coated with gold–palladium.

for these studies were prepared on a TEM grid. Typical micrographs of Nb nanowires are shown in Fig. 4a and b. It is clear from Fig. 4a that Nb wire is polycrystalline. It consists of randomly oriented 3- to 7-nm grains. Lattice fringes have a spacing of $\sim$0.24 nm, which corresponds to the (111) lattice planes of Nb.

A thin, $\sim$2-nm layer near the edges of the wire does not show any crystalline structure. This layer is probably an amorphous oxide formed on the surface because the wire was exposed to the atmosphere. To prevent Nb oxidation, all samples used for transport measurements

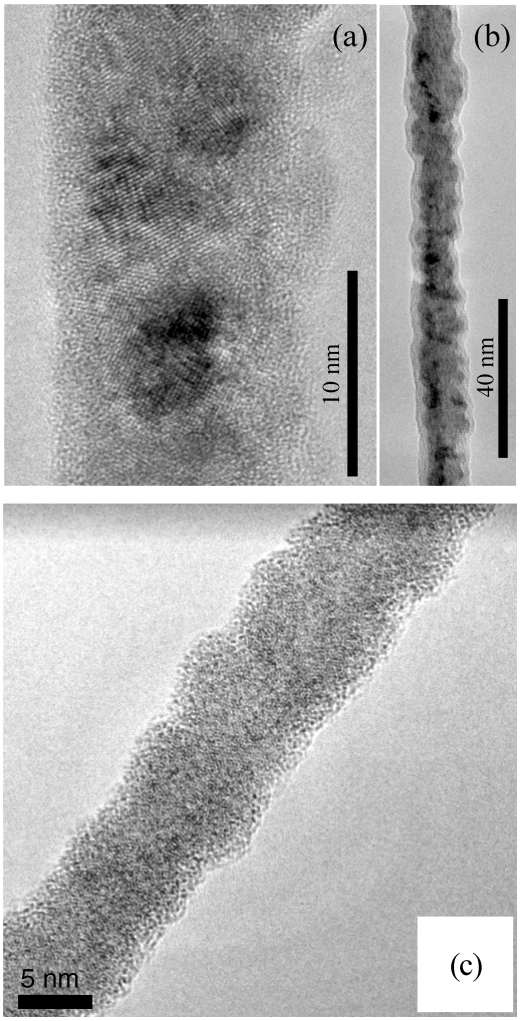

Fig. 4 (a) A high-resolution TEM (JEOL 2010) image of a Nb nanowire fabricated by sputter deposition of a 6-nm Nb film over a carbon nanotube. (b) Image of a Nb nanowire (4 nm of Nb) covered with a protective layer of Si (2 nm). (c) A TEM (JEOL 2010F) micrograph of an amorphous MoGe wire produced by sputter deposition of 7-nm MoGe film (with no Si) over a fluorinated carbon nanotube. The scale bar is 5 nm. The surface ($\sim$1.5 nm) of the wire appears oxidized but the core is intact.

were sputter-coated with a 2-nm-thick Si film. The image of such a wire, protected with Si, is shown in Fig. 4b. The layer of Si (light layer at the surface) produces a uniform coverage of the Nb core (darker center). A typical micrograph of a MoGe nanowire is shown in Fig. 4c. The wire appears amorphous. The width variation of Nb wires (3 nm) appears larger and it has a longer characteristic length scale (along the wire) compared to MoGe wires.

TRANSPORT MEASUREMENTS

Setup and Resistance Measurements

In order to measure voltage vs. current, $V(I)$, curves of a nanowire, a sinusoidal a.c. current (at 12.7 Hz frequency and 1–10 nA amplitude) is injected through a pair of outer electrodes (Fig. 2c) and the voltage is measured on the inner electrodes, using a low-noise PAR 113 amplifier. The current is taken from the high-precision-function generator (Stanford Research Systems, DS 360) connected in series with a 1-MΩ resistor. The fifth electrode (Fig. 2c) is used to measure the resistance of the film electrodes, without involving the wire. The zero-bias resistance is determined from the slope of the best linear fit to the $V(I)$ curves measured at low currents (1–10 nA). The temperature is measured using a Lakeshore calibrated thermometer, Cernox®. The leads connecting the sample to the room temperature amplifiers were made from a Teflon-coated resistive alloy wire, Stablohm 800, produced by California Fine Wire Co. Before reaching the sample, the wire is rolled over a cold Cu rod and coated with a layer of a conducting silver paste. Such an environment helps to thermalize the signal leads and acts as an external, microwave radiation filter (which helps to suppress the room temperature blackbody radiation propagating through signal leads). All electrical leads coming to the sample are additionally filtered with room temperature pi filters (BLP-1.9 from http://www.minicircuits.com). The measurements were done in an He-3 cryostat or in a pumped He-4 Dewar.

An example of a resistance vs. temperature, $R(T)$, curve is shown in Fig. 5. Because the wire is connected in series with some sections of the electrodes (Fig. 2c), two resistive transitions are observed. The first one (at $\sim$6 K) is due to the electrodes and the second transition (at $\sim$3.5 K) is due to the nanowire itself. Thus, the critical temperature of the nanowire is suppressed[39] compared to the film of the same thickness (i.e., the electrodes). The normal-state resistance of the wire, R_N, is determined right below the superconducting transition of the leads, as shown by an arrow in Fig. 5.

Resistivity of Metallic Nanowires

It is important to determine the resistivity of the metal forming the nanowire and compare this to the known bulk values. The resistivity of the wire and its normal resistance should satisfy the following relation:

$$wt = \rho(L/R_N) + A_0 \quad (5)$$

Here R_N is the normal resistance of the nanowire, L is the length measured with SEM, t is the known thickness of

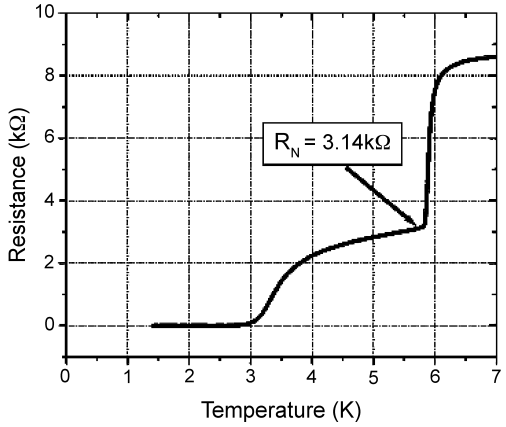

Fig. 5 A typical resistance vs. temperature curve for a MoGe nanowire. The first resistance drop is due to the electrodes and the second, broadened, transition is due to the nanowire. The normal-state resistance of the wire is measured at a temperature slightly lower than the critical temperature of the electrodes, as shown by the arrow.

the sputtered film, w is the apparent width of the wire measured in SEM, and A_0 is the expected area of the insulating material on the surface of the wire, including an oxidized layer and/or protective Si or Ge layers, if any. It is necessary to include the ''dead layer'' area, A_0, in Eq. 5 because the width, w, is not the width of the conducting core of the wire, but is the total width, which is observed in SEM. In Fig. 6, we plot the total area of the nanowire, wt, vs. the unit length conductance, L/R_N. Three groups of points correspond to Nb wires (filled squares), unprotected MoGe wires (open circles) and Ge-coated MoGe wires from Ref. [11] (filled circles). The dependence is linear for each group of samples. The resistivities estimated from the best linear fits (Fig. 6) are $\rho = 4.2 \times 10^{-7}$ Ω m for Nb wires, $\rho = 2.35 \times 10^{-6}$ Ω m for unprotected MoGe wires, and $\rho = 2.46 \times 10^{-6}$ Ω m for protected MoGe wires. This should be compared to bulk resistivity of MoGe, $\rho_{\mathrm{MoGe,BULK}} = 1.6 \times 10^{-6}$ Ω m[25] and to thin film resistivity for Nb: $\rho_{\mathrm{Nb,THINFILM}} = 2.4 \times 10^{-7}$ Ω m.[40] The resistivity of wires is slightly larger but of the same order of magnitude.

This indicates that the wires are continuous and contain no breaks or tunnel barrier between grains. The effective ''dead area'' is $A_0 \approx 14.6$ nm^2 for unprotected MoGe wires, $A_0 \approx 38.8$ nm^2 for Ge-protected MoGe wires, and $A_0 \approx 40$ nm^2 for Nb samples. Protected MoGe samples show a larger A_0 because Ge on their surface contributes to the total width, w. It appears that such protection is not really necessary because the unprotected wires show a lower resistivity and thinner dead layer. In general, the following factors may contribute to large A_0 values: 1) oxidation, 2) presence of a protective layer, 3) wire morphology, presence of grains on the surface, fluctuations of the wire width, and thickness, and 4) a limited resolution of SEM causing some smearing of the images.

Superconductivity in MoGe Nanowires

Parameters of studied amorphous $Mo_{79}Ge_{21}$ nanowires of short length ($L = 100$–150 nm) and various diameters are given in Table 1.

Resistance vs. temperature plots (Fig. 7a) show two different types of behavior: superconducting and insulating. Samples A through F and sample X show a superconducting behavior, i.e., their resistance decreases with temperature. Samples G through J exhibit an increasing resistance (with cooling) and thus considered insulating. Such dichotomy is an indication of an SI quantum transition.[35] The insulating samples not only show a slight increase of their resistance with cooling but also, unlike superconducting wires, they exhibit a maximum of the differential resistance at zero bias current (not shown). The SI transition happens when the normal resistance of the nanowire reaches the quantum resistance $R_Q = h/4e^2 \approx 6.5$ kΩ. Fig. 7a and the inset clearly show that all wires with $R_N < 6.5$ kΩ are superconducting, whereas all others are insulating. This same behavior was found in similar MoGe wires in Ref. [11] in which case the wires were grown on regular (not fluorinated) nanotubes and were protected with 1.5 nm of Ge. Note again that only ~100-nm-long wires are being considered.

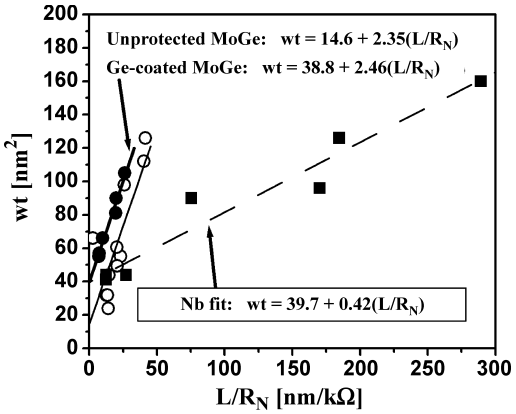

Fig. 6 Cross-section area of the wire, wt, is plotted vs. the unit length conductance, L/R_N. Here w is the width of the nanowire measured under SEM and t is the nominal thickness of the sputtered film. Each data point corresponds to a different sample. Filled squares represent Nb wires, open circles, unprotected MoGe wires, and filled circles, MoGe wire protected with a 1.5-nm Ge film. The best linear fits are shown and the parameters of the fits are indicated on the graph: dashed line for Nb, thick solid line for MoGe wires covered with 1.5 nm of Ge, and thin solid line for plain MoGe nanowires.

Table 1 Parameters of unprotected MoGe wires deposited over fluorinated single-wall carbon nanotubes

Sample	L (nm)	w (nm)	D_{CALC} (nm)	t (nm)	R_N (kΩ)
A	99±10	21±3	11.1	8.5	2.39
B	127±10	19±3	11	8.5	3.14
C	93±10	17±2	8.8	8.5	3.59
D	109±12	13±3	8.3	7.0	4.73
E	116±12	12±4	7.9	7.0	5.61
F	125±7	14±4	7.8	7.0	6.09
G	105±8	11±2	6.2	5.5	8.22
H	121±14	9±2	6.5	5.5	8.67
I	140±9	11±2	6.6	5.5	9.67
J	86±15	14±3	3.1	7.5	26.17

The length of the wire, L, and the width, w, are measured under SEM. The parameter R_N is the normal state resistance, t is the thickness of the sputtered film, and the diameter D_{CALC} is calculated from R_N and L as $D \equiv \sqrt{(4/\pi)(\rho L/R_N)}$, with $\rho = 2.35 \times 10^{-6}$ Ω m.

An SI transition was also observed in Ref. [19] but in that work the transition has been seen when the film square resistance (defined as $R_W = \rho/d$, with ρ being the resistivity of the metal and d the film thickness) reached a critical value close to R_Q. On the contrary, in our case the film square resistance at the SI transition is much lower than R_Q because $R_W \approx R_N(w - \sqrt{A_0})/L \approx 600\ \Omega \ll R_Q$. The total resistance (or perhaps the wire diameter) appears to be a more plausible control parameters driving the transition. Fig. 7b presents all ~100-nm-long samples, including those of Ref. [11] Here the resistance divided by the length of the wire is plotted vs. the temperature normalized by the critical temperature of the film electrodes of each sample. A clear dichotomy confirms the existence of a superconductor–insulator transition.

Now we compare the $R(T)$ curves of superconducting MoGe samples with the LAMH theory. Fig. 8 shows $R(T)$ plots for samples A, B, and C (From Fig. 7a) together with the LAMH fits computed using Eq. 1a. The fits show

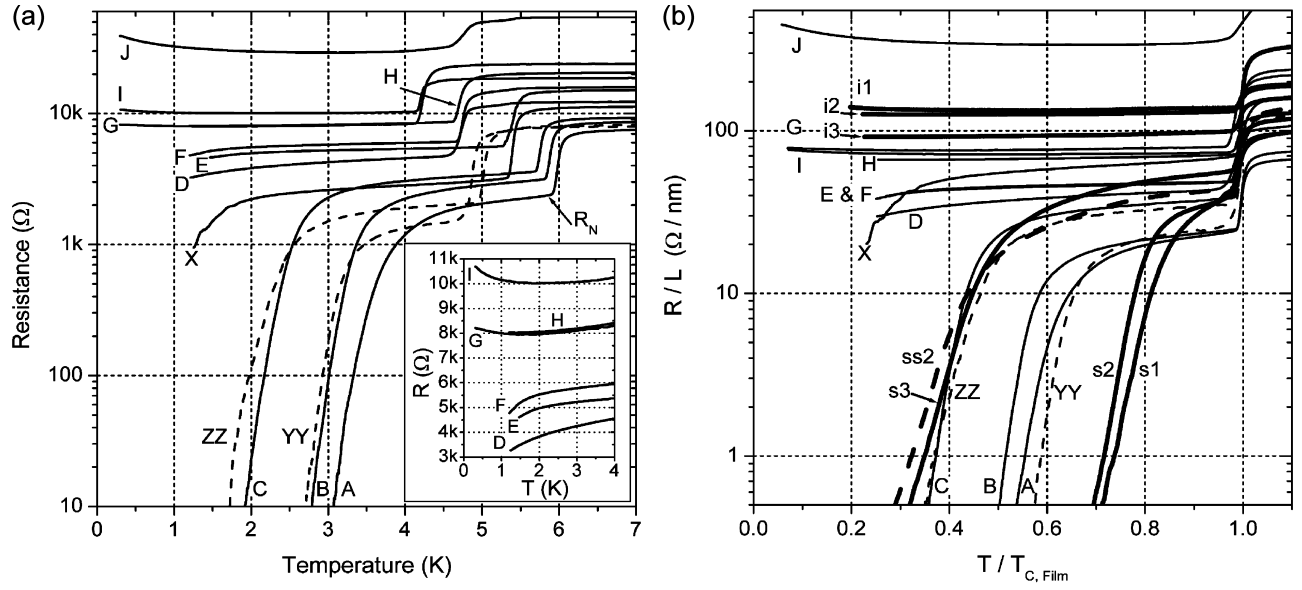

Fig. 7 Resistance vs. temperature of MoGe nanowires. Each curve represents a different sample. (a) Log-linear plots of zero bias resistance vs. temperature. The dashed curves represent double-wire structures. (Inset) The same $R(T)$ data magnified near R_Q. (b) Resistance divided by the length is plotted vs. the temperature normalized by the critical temperature of the film. This combined plot includes all samples listed in Table 1 and the samples from Ref. [11] (thicker lines). The sample X, with $L \approx 50$ nm, is twice shorter than others. A pronounced dichotomy is observed.

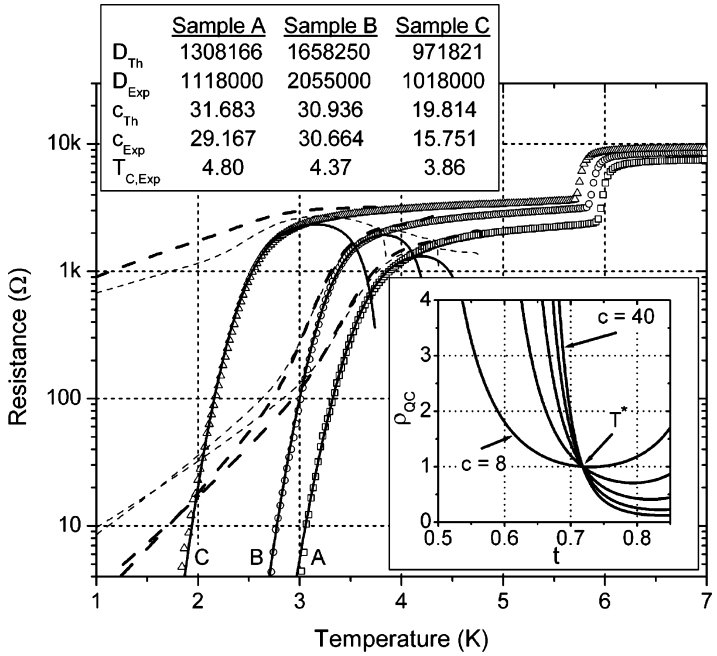

Fig. 8 $R(T)$ data (open symbols) for samples A, B, and C compared to the LAMH theory of TAPS (continuous lines). The table shows the best LAMH fitting parameters c_{Exp}, D_{Exp}, and T_{C} and compares them to the parameters (c_{Th} and D_{Th}) computed from Eqs. 2 and 3. The dashed lines show the predictions of the Giordano model (Ref. [12]) that includes quantum phase slips (heavy dashed lines: $a=1.3$, $B=7.2$; light dashed lines: $a=1$, $B=1$). The coefficients a and B are defined in Ref. [12] and determine the ratio of attempt frequencies and the energy barriers for QPS and TAPS. (Inset) Computed plots of $\rho_{\mathrm{QC}} \equiv R_{\mathrm{MQT}}/R_{\mathrm{LAMH}}$ vs. $t \equiv T/T_{\mathrm{C}}$ for $c=8$, 16, 24, 32, and 40 (assuming $a=1$ and $B=1$). The temperature $T^*=0.718T_{\mathrm{C}}$ is a universal temperature below which the Giordano model predicts a higher QPS rate compared to TAPS.

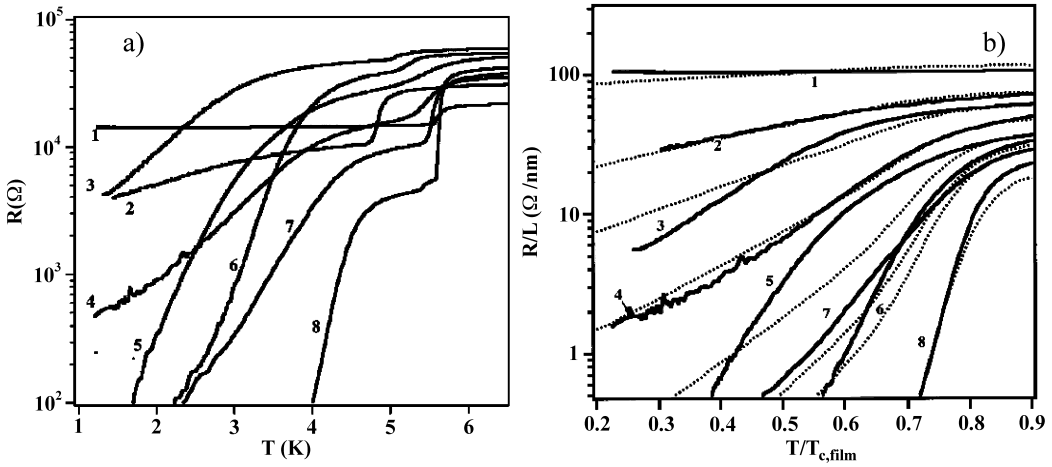

Fig. 9 (a) Resistances vs. temperature for longer (up to 1000 nm) MoGe wires reproduced from Ref. [12] The wire's normal-state resistances and lengths are 1: 14.8 kΩ, 135 nm; 2: 10.7 kΩ, 135 nm; 3: 47 kΩ, 745 nm; 4: 17.3 kΩ, 310 nm; 5: 32 kΩ, 730 nm; 6: 40 kΩ, 1050 nm; 7: 10 kΩ, 310 nm; 8: 4.5 kΩ, 165 nm. (b) Resistance divided by the length plotted vs. temperature, normalized by the critical temperature of the film electrodes. The solid lines represent the data. The dotted lines are calculated using the model of quantum phase slips (see Eq. 4 and Eq. 3 of Ref. [12]). The two fitting parameters that produced the best agreement with the experiment curves are $a=1.3$ and $B=7.2$ used for the entire family of experimental curves.

nearly perfect agreement with the experiment (except very near T_C where the LAMH theory does not work:[27]). The experimental fitting constants c_{Exp} and D_{Exp} are in good agreement with Eqs. 2 and 3. Thus, the wires act as homogenous 1-D superconductors, well described by the LAMH, without including QPS.

Experiments with considerably longer wires (up to 1000 nm) give significantly different results.[12] The dichotomy representing the superconductor–insulator transition was not observed in these longer wires. On the contrary, a smooth crossover from strongly superconducting to weakly superconducting wires has been seen (Fig. 9). It was possible to fit the entire series of $R(T)$ curves of Fig. 9 using only two fitting parameters. The fitting procedure is explained in detail in Ref. [12]. The fits (dashed lines in Fig. 9b) are made using Eq. 4. The coefficients a and B are unknown and were used as free fitting parameters. The coefficient c is defined in Eq. 2. It represents the height of the barrier for the phase slips and it is the same parameter for TAPS as well as for QPS.

The same fitting procedure was applied to short MoGe wires with $R_N<R_Q$ (Fig. 8). The fits, computed using Eq. 4, are shown by dashed lines in Fig. 8. They deviate from the experimental points considerably. Thus we conclude that in short wires with low enough normal state resistance (possibly defined as $R_N<R_Q$) a new regime is realized. This regime can be called ''true'' superconductivity because the QPS rate is strongly suppressed and the LAMH theory gives correct predictions. This theory predicts that resistance should be zero at zero temperature. On the contrary, the wires that show finite contribution of QPS (such as those shown in Fig. 9) should have a nonzero resistance even at zero temperature.

The reason for different behavior in short and long wires is not well understood. Nevertheless, it might be significant that all long wires (Fig. 9) had their normal resistance above R_Q, whereas the superconducting wires (Figs. 7 and 8) have their normal resistance lower than R_Q. Thus, the above-mentioned short and long wires could simply be on different sides of the SI transition. In general, we find that the low-resistance wires show good agreement with the LAMH theory, whereas the highly resistive wires (i.e., those with $R_N>R_Q$) show a considerable deviations form the LAMH (Fig. 9) or even act as insulators (samples G–J, Fig. 7a), possibly due to QPS.

Superconductivity in Nb Nanowires

Nanowires of Nb, grown on fluorinated carbon nanotubes, have properties similar to MoGe nanowires. Parameters of Nb samples are given in Table 2. All Nb wires were protected with a 2-nm Si film. As in MoGe samples, the resistance vs. temperature curves show two transitions (Fig. 10). The first one is due to the Nb film electrodes. Expectedly, this film transition temperature is lower for thinner films.[39] The resistance measured slightly lower than the film transition is taken to be the normal-state resistance of the wire, R_N. The second resistive transition is due to the nanowire itself. The LAMH theory fits, made using Eq. 1a (Fig. 10, continuous lines), demonstrate very good agreement with the data (open circles). The dashed curves in Fig. 10 represent the Giordano model and include the QPS effect, calculated with Eq. 5.

They deviate from the experimental points. The effect of quantum phase slips is negligibly low, i.e., much lower than the Giordano model predicts. Thus, similar to MoGe wires, $\sim$100-nm-long Nb wires show very strong suppression of QPS and good agreement with LAMH. The coherence length, extracted from the LAMH fitting procedure, is $\xi(0)\approx 8$ nm for samples Nb2 and Nb3. This is comparable to $\xi(0)\approx 7$ nm found in sputtered Nb thin films. It also agrees well with the estimate $\xi(0)\approx(\xi_0 l)^{1/2}=$ 6.9 nm, where $\xi_0=40$ nm is the coherence length for clean Nb, and $l\approx 1.2$ nm is the mean free path. For higher resistance samples $\xi(0)\approx 15\div 20$ nm, probably due to the suppression of the critical temperature.

Interestingly, all Nb wires that show good agreement with LAMH satisfy the condition $R_N<R_Q$. The only wire

Table 2 Parameters of Nb nanowires

Sample	R_N (Ω)	L (nm)	t (nm)	w (nm)	T_C (K)	$\xi(0)$ (nm)
Nb1	470	137	8	20	5.8	8.5
Nb2	650	120	7	18	5.6	8.1
Nb3	1610	172	6	16	2.65	18.1
Nb4	2350	177	6	15		
Nb5	4250	110	4	11.5	2.6	16.5
Nb6	9500	113	4	10.3	1.9	16.05
Nb7	15700	196	4	11		
Nb8	47500	235	4	11		

Parameters include the length, L (measured under SEM), the sputtered film thickness, t, the apparent width, w (measured under SEM), and the normal-state wire resistance, R_N. The critical temperature, T_C, and the coherence length, $\xi(0)$, are obtained from the LAMH best fits.

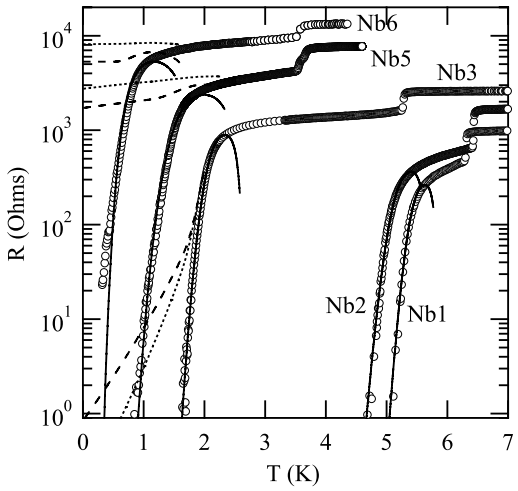

Fig. 10 Temperature dependence of the resistance of Nb nanowires. The experimental points are given by open circles. The solid lines show the fits to the LAMH theory of thermally activated phase slips. These fits are made without including the quantum phase slips. The fitting parameters, $\xi(0)$ and T_C, are indicated in Table 2. The dotted and dashed curves show the fits calculated under the assumption that quantum phase slips do occur. The dashed curves are calculated using generic fitting constants $a=1$ and $B=1$, using Eq. 4. The dotted lines represent the constant obtained in Ref. [12], i.e., $a=1.3$ and $B=7.2$. The other parameters are the same as obtained from LAMH fits.

that deviates from LAMH (sample Nb6) satisfies $R_N > R_Q$. Thus, again, the quantum resistance appears as a critical point. Examples of SI transitions with a critical point at $R_{ENV}=R_Q$ have been studied previously in different systems.[41,42] Such transitions are called dissipative phase transitions (DPT) and are controlled by the resistance of the environment. Typically, a transition into an insulating state takes place when the resistance of the environment (e.g., a shunting resistance) reaches $\sim R_Q = 6.5\ k\Omega$. In short MoGe and Nb nanowires there are certain similarities to the DPT, in particular the fact that deviations from LAMH occur when the normal resistance approaches 6.5 kΩ. The dissipative environment for the nanowires could be the bath of normal electrons generated by phase slips in the nanowire itself. Thus, our preliminary conclusion is that such suppression of QPS is due to a quantum dissipation effect, i.e., the DPT. This question certainly requires further investigation.

High-Bias Current Phenomena in Nanowires

Voltage vs. current measurements, $V(I)$, are presented below for a typical Nb nanowire, Nb2. With decreasing temperature, the $V(I)$ undergoes the following transformations. Slightly below T_C and at high-bias currents, the $V(I)$ follows the exponential dependence predicted by the LAMH theory, $V(I) \sim \exp(I/I_0)$ (Fig. 11a). The experimental value of the coefficient $I_0 \approx 0.09\ \mu A$ is close to the theoretical (Ref. [27] p. 291) value, $I_0 = 2ek_BT/\pi h = 0.06\ \mu A$. At lower T, the resistance becomes immeasurably low until the critical current is reached. At the critical current, the sample shows a few voltage steps (Fig. 11b) and then, at higher bias currents, enters a resistive (or dissipative) regime with a linear $V(I)$. Each new step in the $V(I)$ curve is probably due to an appearance of a new phase slip center (PSC) in the wire.[27]

The multistep $V(I)$ curves indicate that the dissipative size of a single PSC is less than the length of the wire. When temperature decreases further, the steps merge, possibly due to a synchronization of PSCs.[43] At low temperatures, only one large step is present at the critical current and the hysteresis is always observed (Fig. 11c). The hysteresis can be explained either by heating[44] or by the finite relaxation time of the order parameter.[43,45] The heating should not be the dominant effect because the $V(I)$ curves in the dissipative state are linear and parallel to the

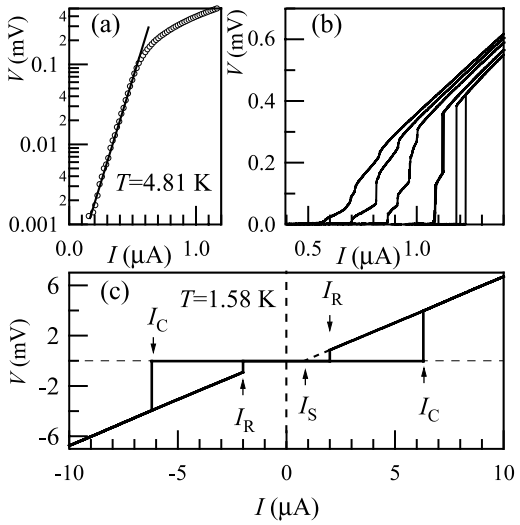

Fig. 11 Voltage vs. current curves measured on one Nb nanowire, Nb2. (a) A $V(I)$ dependence measured at $T=4.8$ K (open circles) in a log-linear representation. The straight solid line is a guide to the eye. (b) A family of $V(I)$ curves measured at different temperatures, close to $T_C=5.6$ K. From the left to the right, the temperatures are: 4.76 K, 4.69 K, 4.58 K, 4.45 K, and 4.35 K. Stepwise behavior corresponds to nucleation of phase slip centers. The other tested Nb samples showed similar steps. (None of the MoGe samples showed such steps.) (c) Hysteretic $V(I)$ variation at the lowest temperature, $T=1.58$ K. The critical current, I_C, the ''retrapping'' current, I_R, and the offset current, I_S, are indicated by arrows.

normal-state dependence, $V=R_N I$, but shifted downward. In other words, they show a nonzero offset current, I_S, meaning that the linear par of the $V(I)$ dependence, observed above the critical current, does not extrapolate to zero current, but rather to a positive offset current, I_S. The I_S represents a nonzero average supercurrent existing even at $I>I_C$. This fact suggests that superconductivity survives in some form in the resistive state.

The critical current for the sample Nb2 extrapolated to $T=0$ K is $I_C(0)=8$ μA. This is close to the depairing critical current calculated as $I_{DP}=(92\ \mu\Omega)LT_C/R_N\xi(0)$,[34] using the parameters extracted from the LAMH fit. This expression gives $I_{DP}=12$ μΩ, reasonably close to experimental value, thus confirming the consistency of the $I_C(T)$ and $R(T)$ measurements. Because the measured values of $I_C(T)$ fluctuate slightly (~100 nA) from measurement to measurement, it is reasonable to assume that the critical current is suppressed below the expected depairing current due to the premature switching effect.[27]

Examples of $V(I)$ curves of MoGe wires are shown in Fig. 12. They are similar to Nb, but they never show multiple steps as in Fig. 11b. This is an indication of a better homogeneity of amorphous MoGe wires or, possibly the larger dissipative size of the phase slip centers in MoGe. This conclusion is confirmed by the observation that the differential resistance measured on the resistive part of the $I(V)$ curve (i.e., above the critical current) coincides with the wire's normal resistance. Therefore, the dissipative size of the phase slip center is equal to the wire's length of ~100 nm. The measured critical current of MoGe wires is close to the estimated depairing current and it diminishes with the wire's approaching the SI transition (Fig. 12). Some suppression of the critical current due to premature switching has also been observed.

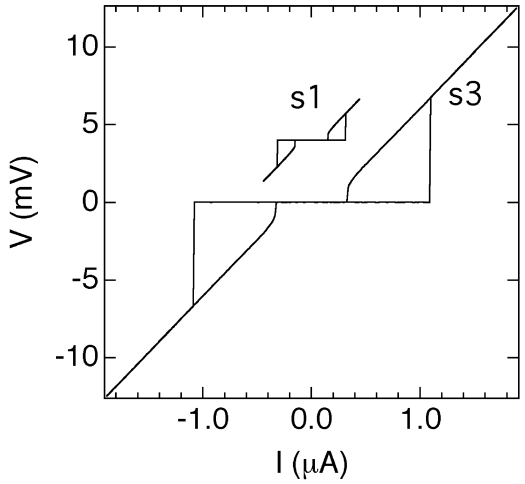

Fig. 12 Voltage vs. current curves for the MoGe samples s1 and s3 (same samples as presented in Ref. [11]). The R–T curves for these samples are plotted in Fig. 8b. The measurement is done at 1.5 K. The sample s1 had a lower critical temperature and higher normal resistance, and was close to the SI transition. Correspondingly, the critical current for s1 is also lower. Yet, the general shape of both curves is similar. Note that the $V(I)$ curve of this sample is shifted vertically for clarity (but not rescaled). Both curves show a nonzero offset current.

CONCLUSION

Suspended molecular templates have been used for the fabrication of sub-10-nm nanowires. This allowed an extensive research of 1-D superconductivity. The main results are: 1) The LAMH theory is tested in a wide range of temperatures and showed very good agreement with measurements carried on short wires (~100 nm), with $R_N<R_Q$. These wires behave as ''true superconductors'' and should approach zero resistance at zero temperature. 2) Deviations from the LAMH are observed on wires with $R_N>R_Q$. The Giordano model, involving quantum tunneling of phase slips, provides good fits for such wires. These wires should have a finite resistance at zero temperature. An insulating behavior is also observed in samples, which are short and satisfy the condition $R_N>R_Q$. Future work will address such issues as the origin of the superconductor–insulator transition and the nature of the insulating state.

ACKNOWLEDGMENTS

This work was supported by NSF carrier grant DMR-01-34770. Part of the work was done in the Center for Microanalysis of Materials, University of Illinois, which is partially supported by the U.S. Department of Energy under grant DEFG02-91-ER45439.

REFERENCES

1. Likharev, K.K. Superconducting weak links. Rev. Mod. Phys. **1979**, *51*, 101–160.
2. Likharev, K.K. *Dynamics of Josephson Junctions and Circuits*; Gordon and Breach: New York, 1986.
3. Chen, W.; Rylyakov, A.V.; Patel, V.; Lukens, J.E.; Likharev, K.K. Rapid single flux quantum T-flip

flop operating up to 770 GHz. IEEE Trans. Appl. Supercond. **1999**, *9*, 3212–3215.
4. Makhlin, Yu.; Schön, G.; Shnirman, A. Quantum state engineering with Josephson-junction devices. Rev. Mod. Phys. **2001**, *73*, 357–400.
5. Averin, D.V. Adiabatic quantum computation with Cooper pairs. Solid State Commun. **1998**, *105*, 659–664.
6. Nakamura, Y.; Pashkin, Y.A.; Tsai, J.S. Coherent control of macroscopic quantum states in a single-Cooper-pair box. Nature **1999**, *398*, 786–788.
7. Orlando, T.P.; Mooij, J.E.; Tian, L.; Van der Wal, C.H.; Levitov, L.; Lloyd, S.; Mazo, J.J. A superconducting vortex qubit. Phys. Rev., B **1999**, *60*, 15398–15413.
8. Orlando, T.P.; Delin, K.A. *Foundation of Applied Superconductivity*; Addison-Wesley: Reading, MA, 1991.
9. Skalare, A.; McGrath, W.R.; Bumble, B.; LeDuc, H.G.; Burke, P.J.; Verheijen, A.A.; Schoelkopf, R.J.; Prober, D.E. Large bandwidth and low noise in a diffusion-cooled hot-electron bolometer mixer. Appl. Phys. Lett. **1996**, *68*, 1558–1560.
10. Giordano, N. Evidence of macroscopic quantum tunneling in one-dimensional superconductors. Phys. Rev. Lett. **1988**, *61*, 2137–2140.
11. Bezryadin, A.; Lau, C.N.; Tinkham, M. Quantum suppression of superconductivity in ultrathin nanowires. Nature **2000**, *404*, 971–974.
12. Lau, C.N.; Markovic, N.; Bockrath, M.; Bezryadin, A.; Tinkham, M. Quantum phase slips in superconducting nanowires. Phys. Rev. Lett. **2001**, *87*, 217003-1–217003-4.
13. Matveev, K.A.; Larkin, A.I.; Glazman, L.I. Persistent current in superconducting nanorings. Phys. Rev. Lett. **2002**, *89*, 096802-1–096802-4.
14. Zaikin, A.D.; Golubev, D.S.; van Otterlo, A.; Zimányi, G.T. Quantum phase slips and transport in ultrathin superconducting wires. Phys. Rev. Lett. **1997**, *78*, 1552–1555.
15. Rafael, G.; Demler, E.; Oreg, Y.; Fisher, D.S. cond-mat/0302498. http://xxx.lanl.gov.
16. Büchler, H.P.; Geshkenbein, V.B.; Blatter, G. Quantum fluctuations in thin superconducting wires of finite length. cond-mat/0306617. http://xxx.lanl.gov.
17. Kociak, M.; Kasumov, A.Yu.; Gueron, S.; Reulet, B.; Khodos, I.I.; Gorbatov, Yu.B.; Volkov, V.T.; Vaccarini, L.; Bouchiat, H. Superconductivity in ropes of single-walled carbon nanotubes. Phys. Rev. Lett. **2001**, *86*, 2416–2419.
18. Smith, R.A.; Handy, B.S.; Ambegaokar, V. Width and magnetic-field dependence of the transition temperature in ultranarrow superconducting wires. Phys. Rev., B **2001**, *63*, 094513-1–094513-12.
19. Xiong, P.; Herzog, A.V.; Dynes, R.C. Negative magnetoresistance in homogeneous amorphous superconducting Pb wires. Phys. Rev. Lett. **1997**, *78*, 927–930.
20. Xiong, P.; Herzog, A.V.; Dynes, R.C. Negative magnetoresistance in homogeneous amorphous superconducting Pb wires. Phys. Rev. Lett. **1998**, *78*, 927–930.
21. Miyazaki, H.; Takahide, H.Y.; Kanda, A.; Ootuka, Y. Quantum phase transition in one-dimensional arrays of resistively shunted small Josephson junctions. Phys. Rev. Lett. **2002**, *89*, 197001-1–197001-4.
22. Rogachev, A.; Bezryadin, A. Superconducting properties of polycrystalline Nb nanowires templated by carbon nanotubes. Appl. Phys. Lett. **2003**, *83*, 512–514.
23. Graybeal, G.M.; Beasley, M.R. Localization and interaction effects in ultrathin amorphous superconducting films. Phys. Rev., B **1984**, *29*, 4167–4169.
24. Yazdani, A.; Kapitulnik, A. Superconductor–insulator transition in two-dimensional a-MoGe thin films. Phys. Rev. Lett. **1995**, *74*, 3037–3040.
25. Graybeal, J.M. *Ph.D. Thesis*; Stanford University: Stanford, CA, 1985.
26. Orlando, T.P.; Delin, K.A. *Foundation of Applied Superconductivity*; Addison-Wesley: Reading, MA, 1991.
27. Tinkham, M. *Introduction to Superconductivity*, 2nd Ed.; McGraw-Hill: New York, 1996.
28. Mermin, N.D.; Wagner, H. Absence of ferromagnetism or antiferromagnetism in one- or two-dimensional isotropic Heisenberg models. Phys. Rev. Lett. **1966**, *17*, 1133–1136.
29. Little, W.A. Decay of persistent currents in small superconductors. Phys. Rev. **1967**, *156*, 396–403.
30. Langer, J.S.; Ambegaokar, V. Intrinsic resistive transition in narrow superconducting channels. Phys. Rev. **1967**, *164*, 498–510.
31. McCumber, D.E.; Halperin, B.I. Time scale of intrinsic resistive fluctuations in thin superconducting wires. Phys. Rev., B **1970**, *1*, 1054–1070.
32. Lukens, J.E.; Warburton, R.J.; Webb, W.W. Onset of quantized thermal fluctuations in ''one-dimensional'' superconductors. Phys. Rev. Lett. **1970**, *25*, 1180–1183.
33. Newbower, R.S.; Beasley, M.R.; Tinkham, M. Fluctuation effects on the superconducting transition of tin whisker crystals. Phys. Rev., B **1972**, *5*, 864–868.

34. Tinkham, M.; Lau, C.N. Quantum limit to phase coherence in thin superconducting wires. Appl. Phys. Lett. **2002**, *80*, 2946–2948.
35. Bollinger, A.T.; Rogachev, A.; Remeika, M.; Bezryadin, A. The effert of morphology on the superconductor-insulator transition in 1-D nanowires. *in press*.
36. Kelly, K.F.; Chiang, I.W.; Michelson, E.T.; Hauge, R.H.; Margrave, J.L.; Wang, X.; Scuseria, G.E.; Radoff, C.; Halas, N.J. Insight into the mechanism of sidewall functionalization of single-walled nanotubes: An STM study. Chem. Phys. Lett. **1999**, *313*, 445–450.
37. Zhang, Y.; Dai, H. Formation of metal nanowires on suspended single-walled carbon nanotubes. Appl. Phys. Lett. **2000**, *77*, 3015–3017.
38. Bezryadin, A.; Dekker, C. Nanofabrication of electrodes with sub-5 nm spacing for transport experiments on single molecules and metal clusters. J. Vac. Sci. Technol., B **1997**, *15*, 793–799.
39. Oreg, Y.; Finkel'stein, A.M. Suppression of Tc in superconducting amorphous wires. Phys. Rev. Lett. **1999**, *83*, 191–194.
40. Park, S.I.; Geballe, T.H. Superconducting tunneling in ultrathin Nb films. Phys. Rev. Lett. **1986**, *57*, 901–904.
41. Penttilä, J.S.; Parts, Ü.; Hakonen, P.J.; Paalanen, M.A.; Sonin, E.B. Superconductor–insulator transition in a single Josephson junction. Phys. Rev. Lett. **1999**, *82*, 1004–1007.
42. Miyazaki, H.; Takahide, Ya.; Kanda, A.; Ootuka, Yo. Quantum phase transition in one-dimensional arrays of resistively shunted small Josephson junctions. Phys. Rev. Lett. **2002**, *89*, 197001-1–197001-4.
43. Tidecks, R. *Current-Induced Nonequilibrium Phenomena in Quasi-One-Dimensional Superconductors*; Springer: Berlin, 1990; 138.
44. Tinkelman, M.; Free, J.U.; Lau, C.N.; Markovic, N. Mysteretic I-V curves of superconducting nanowires. Phys. Rev. B **2003**, *68*, 134515-1–134515-7.
45. Song, Y. Origin of capacitance is superconducting microbridges. J. Appl. Phys. **1976**, *47*, 2651–2655.

Marcel Dekker, Inc.
270 Madison Avenue, New York, New York 10016